https://doi.org/10.5194/tc-2020-8
Preprint. Discussion started: 3 February 2020

The Cryosphere Discussions

Estimating statistical errors in retrievals of ice velocity and deformation parameters from satellite images and buoy arrays

Wolfgang Dierking[1,2], Harry Stern[3], Jennifer K. Hutchings[4]

[1]Center for Integrated Remote Sensing and Forecasting for Arctic Operations, University in Tromsø, 9019 Tromsø, Norway
[2]Alfred Wegener Institute Helmholtz Center for Polar and Marine Research, 27570 Bremerhaven, Germany
[3]Polar Science Center, Applied Physics Laboratory, University of Washington, 1013 NE 40th Street, Seattle, WA 98105, USA
[4] College of Earth Ocean and Atmospheric Sciences, Oregon State University, 104 CEOAS Administration building, Corvallis OR 97331, USA

Correspondence to: Wolfgang Dierking (Wolfgang.Dierking@awi.de)

Abstract. The objective of this note is to provide the background and basic tools to estimate the statistical error of deformation parameters that are calculated from displacement fields retrieved from synthetic aperture radar (SAR) imagery or from location changes of position sensors in an array. We focus here specifically on sea ice drift and deformation. In the most general case, the uncertainties of divergence/convergence, shear, vorticity, and total deformation are dependent on errors in coordinate measurements, the size of the area and the time interval over which these parameters are determined, and the velocity gradients within the boundary of the area. If displacements are calculated from sequences of SAR images, also a tracking error has to be considered. Timing errors in position readings are usually very small and can be neglected. We give examples for magnitudes of position and timing errors typical for buoys and SAR sensors, in the latter case supplemented by magnitudes of the tracking error, and apply the derived equations on geometric shapes frequently used for deriving deformation from SAR images and buoy arrays. Our case studies show that the size of the area and the time interval for calculating deformation parameters have to be chosen within certain limits to make sure that the uncertainties are smaller than the magnitudes of deformation parameters.

1 Introduction

The retrieval of sea ice drift vectors and deformation parameters from pairs or sequences of satellite synthetic aperture radar (SAR) images has gained increased attention during recent years because of the growing availability of suitable data (e.g. Stern and Moritz, 2002; Karvonen, 2012; Berg and Eriksson, 2014; Komarov and Barber, 2014; Lehtiranta, 2015; Muckenhuber et al., 2016; Demchev et al., 2017; Korosov and Rampal, 2017). Sea ice kinematics is also studied based on data from arrays of buoys or GPS receivers (e.g. Lindsay, 2002; Hutchings et al., 2008; Hutchings et al., 2012; Itkin et al. 2017a), which in addition can serve as reference in comparisons to motion vectors obtained from SAR images. The knowledge of spatially detailed motion and deformation fields is potentially useful in ice navigation to locate divergent or compressive ice areas, as complementary information for operational sea ice mapping, for validation of models for forecasting of ice conditions, and for assimilation into ice models (Karvonen, 2012). Such practical applications require that the errors of the retrieved drift and deformation parameters are known. For buoys, errors in drift measurements depend on the accuracy of position and time readings. The accuracy of deformation parameters is not only affected by errors in drift magnitude and direction but also by the size and shape of buoy arrays. Drift vectors derived from pairs of satellite images are the result of correlation techniques or object detections, while deformation parameters are calculated from spatial arrangements of adjacent drift vectors surrounding the area of interest. This means that drift and deformation errors do not only depend on the geolocation accuracy of satellite images but also on the reliability and robustness of the drift retrieval algorithm. In this technical note we focus on the estimation of statistical errors for ice velocity and deformation. The issue of error estimation was repeatedly addressed in the past, scattered in a number of publications and restricted to single aspects related to the respective analysis

https://doi.org/10.5194/tc-2020-8
Preprint. Discussion started: 3 February 2020


The Cryosphere Discussions
Open Access
EGU

(e.g. Lindsay and Stern, 2003; Hollands and Dierking, 2011; Bouillon and Rampal, 2015; Hollands et al., 2015; Linow et al., 2015; Griebel and Dierking, 2018). Our motivation is to provide the mathematical background, together with examples of applications and discussions of validity, in a broader context. We emphasize that here we deal with statistical errors, but not with truncation errors due to discretization as described, e.g. in Lindsay and Stern (2003), Bouillon and Rampal (2015) and Griebel and Dierking (2018). Although this note is specifically focused on retrievals of parameters characterizing sea ice kinematics, the mathematical framework is also applicable, e.g., for movement and deformation of ice shelves and glaciers, or for model simulations of sea ice, glacier, and ice sheet dynamics.

In Sect. 2 we summarize the basics and provide equations for calculating errors of drift and deformation parameters, supplemented with the derivation of general-case uncertainties of divergence, vorticity, shear, and total deformation. The equations are used in Sect. 3 to quantify the influence of different parameters such as geolocation and tracking errors, or shape and size of buoy arrays and grid cells. Conclusions are presented in Sect. 4.

2 Errors of drift and deformation parameters

In this section, we provide a short description of the estimation of errors and the computation of strain rates, and then derive the statistical errors for drift velocity, polygon areas, divergence, shear, vorticity, and total deformation. The statistical errors quantify uncertainties that are introduced by random fluctuations in the measurements. If the random fluctuations are small, data are measured with a high degree of precision, but not necessarily with high accuracy. The latter requires that the measured value is close to the true value, whereas precision refers to the reproducibility of a measurement (Bevington and Robinson, 2003, chapter 1).

2.1 Error propagation and calculation of deformation

The formula for error propagation is based on the splitting method, i.e. the decomposition of a measured variable x into its true value and the measurement error: $x = x_{true} + x_{error}$, where x_{true} is considered to be a constant, and x_{error} is a random variable with expected value $E(x_{error}) = 0$ and variance $E(x^2_{error}) = \sigma^2$. If a quantity Q is calculated from measured variables x_k, i. e. $Q = f(x_1, x_2, \ldots, x_n)$, a Taylor series expansion can be applied to estimate the error of Q. Usually only the linear term is retained:

$$Q = f(x_{1,true}, x_{2,true}, \cdots, x_{n,true}) + \sum_{i=1}^{n} \left[\frac{\partial f}{\partial x_i}(x_{1,true}, x_{2,true}, \cdots, x_{n,true})\right][x_{i,error}] \quad (1)$$

The variance is obtained by moving the first term to the left-hand side, squaring both sides and applying the expected value operator E( ) (Bevington and Robinson, 2003). This operation results in

$$\sigma_Q^2 = \sum_i \left(\frac{\partial f}{\partial x_i}\right)^2 \sigma_i^2 + \sum_{i \neq j} \sum \left(\frac{\partial f}{\partial x_i}\right)\left(\frac{\partial f}{\partial x_j}\right)\sigma_{ij} \qquad i=1,n,\ j=1,n \quad (2)$$

where σ_i^2 is the variance and σ_{ij} the covariance. If we can assume that the errors are uncorrelated, the second term on the right side of (2) is zero. We will use the notation “uncertainty” synonymously with “standard deviation of the absolute error”.

Deformation parameters are calculated from different combinations of the components of the velocity gradient tensor ($\partial u/\partial x$, $\partial v/\partial x$, $\partial u/\partial y$, $\partial v/\partial y$) = (u_x, v_x, u_y, v_y) (Leppäranta, 2011), here given in a Cartesian coordinate system, where $u(x,y)$ and $v(x,y)$ are the velocity components in x- and y-direction at position (x,y). We have

divergence $\dot{\varepsilon}_{div} = u_x + v_y$ (3a)

vorticity $\dot{\varepsilon}_{vrt} = v_x - u_y$ (3b)

https://doi.org/10.5194/tc-2020-8
Preprint. Discussion started: 3 February 2020

shear $$\dot{\varepsilon}_{shr} = \sqrt[2]{(u_y + v_x)^2 + (u_x - v_y)^2}$$ (3c)

and total deformation $$\dot{\varepsilon}_{tot} = \sqrt[2]{\dot{\varepsilon}_{div}{}^2 + \dot{\varepsilon}_{shr}{}^2}$$ (3d)

Divergence and shear are the two invariants of the symmetric deformation tensor. The dimension of $\dot{\varepsilon}$ is velocity change per length unit, hence [time]$^{-1}$. For ease of reference, we briefly repeat the physical meaning of different velocity gradient combinations (after Cuffey and Paterson, 2010; Leppäranta, 2011): Imagine a rectangle with its sides L_x and L_y parallel to the x and y-axes of a 2D Cartesian coordinate system. In this case the gradients u_x, v_y are normal strain rates, leading to an extension or contraction of the rectangle in the respective direction. The normal strain along the x-axis, e.g., is $\Delta L_x(t) / L_x = u_x \Delta T$. Here ΔT is the time interval $\Delta T = t - t_0$ during which the effect of deformation is analyzed, and $L_x+\Delta L_x$ is the side length at time $t_0+\Delta T$. The sum $u_x + v_y$ is the divergence or convergence, dependent on the sign. The expression $u_y + v_x$ is linked to the change of shape of the rectangle (pure shear). The normal shear, $u_x - v_y$, quantifies the change in length difference between the sides of the rectangle. The vorticity ($v_x - u_y$), which is twice the rotation rate, describes the rotation about an axis vertical to the x-y plane (positive counterclockwise) without change of shape. Let the rectangle be located in a temporally constant velocity field with, e.g., u_x=0.1d^{-1}, v_y=0.05d^{-1}, u_y=0, v_x=0, then the divergence is $\dot{\varepsilon}_{div} = 0.15$ d^{-1} = 15% d^{-1}. Assuming that the sides of the rectangle are L_x and L_y at time t_0, its area $A_0 = L_x L_y$ increases to $(L_x + u_x L_x \Delta T)\,(L_y + v_y L_y \Delta T) = A_0\,(1+ u_x \Delta T)(1+v_y \Delta T) = 1.155 A_0$ for ΔT = 1 day. Since only the difference u_x-v_y contributes to the square root (3c), $\dot{\varepsilon}_{shr}$ =0.05d^{-1}=5% d^{-1} is the normal shear (Hutchings et al., 2012).

The deformation of a region R (covered by the buoy array or grid cell) with area A is calculated from the *spatial averages* of the velocity gradient components over the region. For the u_x component, for example, the corresponding expression is (Thorndike, 1986):

$$\overline{u_x} = \frac{1}{A}\iint_R \frac{\partial u}{\partial x} da = \frac{1}{A}\oint_C u\, \boldsymbol{n}\, \boldsymbol{e_x}\, dl \quad (4)$$

Here da and dl are the differentials for area and length, $\boldsymbol{n}$ is the outward normal vector to the perimeter C of R, and $\boldsymbol{e_x}$ is the unit vector in x-direction. This is Green's theorem, which relates a line integral along a closed curve C to the area integral over a plane region R bounded by C. The application of the theorem requires that the velocity components u and v have continuous first-order partial derivatives on R. Our calculations of strain rate components in a Cartesian coordinate system are carried out using

$$u_x = \frac{1}{A}\oint_C u\, dy \cong \frac{1}{2A}\sum_{i=1}^{n}(u_{i+1} + u_i)\,(y_{i+1} - y_i) \quad (5)$$

and the other components of the velocity gradient tensor accordingly. This expression comes from the trapezoid rule for integration, taking n points around the perimeter of R, where $(u_{i+1} + u_i)/2$ is the estimate of u on the i^{th} segment, and $(y_{i+1} - y_i)$ is dy. In (5), i is the summation index which traces the boundary in a counterclockwise sense, n is the number of vertices for the grid cell (or number of buoys), and A is the area of the grid cell (or of the polygon spanned by the buoy array). Here, $u_{n+1} \equiv u_1$ and $y_{n+1} \equiv y_1$ (closed polygon). In Eq. (5) we have omitted the overbar. The strain rate is implicitly an average over A. This is also valid for Eqs. (3a) – (3d).

The velocity vectors may be obtained from an array of buoys, where the buoys' positions are regarded as the vertices of a polygon. The displacement of a buoy is usually calculated from the distance between distinct positions, and the velocity is determined as the displacement divided by the time period between position fixes. When using pairs of satellite images, sea ice deformation is obtained from the displacements of recognizable structures or patterns in these images. These are referred to as ice structures from here on. In the reference image, a grid can be constructed by connecting the center positions of adjacent

https://doi.org/10.5194/tc-2020-8
Preprint. Discussion started: 3 February 2020

ice structures by lines. If movements of single ice structures differ between acquisitions of image 1 and image 2, the shapes and sizes of grid cells have changed in the second image. It is the presence of velocity gradients due to locally varying physical forces that causes the deformation. In practice the movement of sea ice is obtained using different methods (e.g. Holt et al., 1992; Stern and Moritz, 2002; Karvonen, 2012; Muckenhuber et al., 2016; Korosov and Rampal, 2017), which determine the spatial distribution and density of the displacement vectors. The vectors can be regularly spaced on the crossing points of horizontal and vertical grid lines as a result of pattern matching algorithms in an Eulerian approach, or they can be irregularly distributed, which is typical for the Lagrangian approach applied in feature or buoy tracking, see Fig. 1.

The errors discussed in the following subsections can be traced back to errors in the position of reference points (i.e. vertices of a grid, or buoys). Lindsay and Stern (2003) denote this error type as geolocation error. On a horizontal plane two coordinates (e. g x, y or latitude, longitude) determine the positions of the start and end points of the displacement, respectively. The distance $d = \sqrt[2]{(x'-x)^2+(y'-y)^2}$ is prone to the errors of the coordinate readings. Its uncertainty is $\sigma_d^2 = 2\sigma_{coord}^2$, assuming $\sigma_{coord} = \sigma_x = \sigma_y = \sigma_{x'} = \sigma_{y'}$, and no correlation between coordinate measurements at the end points, see Eq. (2). When displacements are retrieved from a pair of SAR images, one needs to consider position and tracking uncertainties σ_{coord}^2 and σ_{tr}^2. The latter arises from the fact that in a satellite image details of structures on pixel scale may be difficult to match between images 1 and 2. In this case the uncertainty in displacement (which here is the distance between positions of an ice structure in images 1 and 2) is $\sigma_d^2 = 2\sigma_{coord}^2+\sigma_{tr}^2$. For buoy arrays, σ_{tr}^2 is zero, since a buoy remains fixed relative to the ice floe on which it was deployed. The assumption of independent geolocation errors may not be valid if distances between moving objects are small. Holt et al. (1992) give a correlation length of 10 km for the geolocation error, σ_{coord}. If, e.g., the distance between two moving objects is closer than this, the position errors cancel and $\sigma_d^2 = \sigma_{tr}^2$ for the retrieval from a SAR image pair and $\sigma_d^2 = 0$ between two buoys. Hence within a circle of 10km or less in diameter, deformation can be estimated with sufficient accuracy even if geolocation errors are high. It should be considered, however, that the correlation length depends on the measurement system.

2.2 Uncertainty of drift velocity

The deformation is calculated from components of the ice drift velocity vectors according to Eq. (5). Hence, we have to consider the uncertainty in the measurements of velocity components u_i and v_i. The components are calculated from $u = d_x/\Delta T$ and $v = d_y/\Delta T$, where $d_x = (x' - x)$ and $d_y = (y' - y)$ are the displacements in x- and y-direction, respectively, and ΔT is the time interval needed for the position change from (x, y) to (x', y'). Considering that errors in measuring time and positions are not correlated, we obtain from Eq. (2), taking into account a possible tracking error:

$$\sigma_u^2 = \frac{1}{\Delta T^2}\sigma_{d_x}^2 + \left(\frac{-d_x}{\Delta T^2}\right)^2 \sigma_{\Delta T}^2 = \frac{1}{\Delta T^2}(2\sigma_x^2 + \sigma_{tr_x}^2 + u^2\sigma_{\Delta T}^2) \quad (6a)$$

$$\sigma_v^2 = \frac{1}{\Delta T^2}\sigma_{d_y}^2 + \left(\frac{-d_y}{\Delta T^2}\right)^2 \sigma_{\Delta T}^2 = \frac{1}{\Delta T^2}(2\sigma_y^2 + \sigma_{tr_y}^2 + v^2\sigma_{\Delta T}^2) \quad (6b)$$

where σ_{d_x}, σ_{d_y} are the uncertainties of the displacements (distances) in x- and y-direction, and σ_{tr_x}, σ_{tr_y} are the corresponding components of the tracking error. If the uncertainty in timing, $\sigma_{\Delta T}^2$ is not zero, the assumption that $\sigma_u^2 = \sigma_v^2$ is only valid if $u^2 = v^2$. The uncertainty in speed U (i. e. the magnitude of velocity vector $\mathbf{U}$) can be computed using Eq. (6), replacing σ_u^2 with σ_U^2, $\sigma_{d_x}^2$ with σ_d^2, $\sigma_{tr_x}^2$ with σ_{tr}^2, and u with U, considering that $U = \sqrt[2]{u^2+v^2}$, and $d = \sqrt[2]{(x'-x)^2+(y'-y)^2}$. When calculating the relative error variance σ_U/U, one obtains Eq. (A1) in Hutchings et al. (2012).

If, on the other hand, both components of the vector $\boldsymbol{U}$ are determined separately (hence considering magnitude and direction), the result is different:

https://doi.org/10.5194/tc-2020-8
Preprint. Discussion started: 3 February 2020

$$\sigma_U^2 = \left(\frac{\partial U}{\partial u}\right)^2 \sigma_u^2 + \left(\frac{\partial U}{\partial v}\right)^2 \sigma_v^2 = \left(\frac{u}{U}\right)^2 \sigma_u^2 + \left(\frac{v}{U}\right)^2 \sigma_v^2 \quad (7)$$

Substituting Eq. (6) for σ_u^2 and σ_v^2 and setting $\sigma_{dx}^2 = \sigma_{dy}^2 = 2\sigma_{coord}^2 + \sigma_{tr}^2$ yields

$$\sigma_U^2 = \frac{2\sigma_{coord}^2 + \sigma_{tr}^2}{\Delta T^2} + \frac{\sigma_{\Delta T}^2}{\Delta T^2}\left(\frac{u^4+v^4}{u^2+v^2}\right) \quad (8)$$

If $\sigma_{\Delta T}$ cannot be neglected, and if u=0 and v=U or v=0 and u=U, the second term of Eq. (8) yields $U^2(\sigma_{\Delta T}^2/\Delta T^2)$, which is the uncertainty in speed given above. If, on the other hand, u=v and hence U^2=2u^2, the second term is $0.5U^2(\sigma_{\Delta T}^2/\Delta T^2)$. This result may be viewed as if independent measurements of the two components u and v reduce the uncertainty contribution of $\sigma_{\Delta T}^2$.

2.3 Uncertainty of polygon area

The uncertainty of an area measurement is needed for application of Eq. (5) and equations presented in the following sections. The starting point for calculating the variance of error for the measurement of an area is the Surveyor's Area Formula valid for a polygon with an outline consisting of n segments in a plane spanned by the x- and y-axis:

$$A = \frac{1}{2}\sum_{i=1}^{n}(x_i\, y_{i+1} - x_{i+1} y_i) \quad (9)$$

Here $x_{n+1} \equiv x_1$ and $y_{n+1} \equiv y_1$ (closed polygon), i is the summation index, and the boundary is traced in a counterclockwise sense. We have to consider that each coordinate appears twice in the sum of Eq. (9). When i=k we have, e.g. for x: $x_k y_{k+1}$, and when i=k-1 we have $-x_k y_{k-1}$. For the law of error propagation we need the derivatives:

$$\frac{\partial A}{\partial x_k} = \frac{1}{2}(y_{k+1} - y_{k-1}) \quad \text{and} \quad \frac{\partial A}{\partial y_k} = -\frac{1}{2}(x_{k+1} - x_{k-1}) \quad (10)$$

where k is the index of the derivative. Hence, we obtain

$$\sigma_A^2 = \frac{1}{4}\sum_{i=1}^{n}\left[\sigma_{i\_x}^2 (y_{i+1} - y_{i-1})^2 + \sigma_{i\_y}^2 (x_{i+1} - x_{i-1})^2\right] \quad (11)$$

We can assume that coordinate uncertainties $\sigma_{i\_x}^2 = \sigma_{i\_y}^2 = \sigma_{coord}^2$ are equal and the same for all measured positions. The uncertainty of the area is then

$$\sigma_A^2 = \frac{\sigma_{coord}^2}{4}\sum_{i=1}^{n}[(y_{i+1} - y_{i-1})^2 + (x_{i+1} - x_{i-1})^2] \quad (12)$$

Examples of applying Eq. (12) on basic polygons are shown in Fig. 2. Arbitrarily shaped triangles and quadrangles, which are basic patterns for arrays of three or four buoys and for grid cells in satellite images when applying the Lagrangian approach, are shown at the bottom. The x-y coordinate system is here oriented such that the calculation of the uncertainty is easy. For any orientation of the triangle or quadrangle, side lengths and distances can be derived from the coordinates (x, y) of the edge points. For squares and equal-sided right-angled triangles, which are typical grid cells when retrieving ice drift from satellite

https://doi.org/10.5194/tc-2020-8
Preprint. Discussion started: 3 February 2020

images in a Eulerian approach, the uncertainty is directly proportional to the area. If a square grid cell is split into two triangles (as in Fig. 1), the uncertainty in area of each triangle is half that of the square.

For an assessment on how the polygon shape affects the magnitude of uncertainty we require that the enclosed area remains constant. The areas of a square with side length L and a right-angled triangle with two sides of length L_T are equal if $L_T = \sqrt{2}L$. In this case we get $\sigma_A^2 = 2\sigma_{coord}^2 L^2$ for both square and triangle, which means that in this particular case the increase in number of vertices does not result in a decrease of σ_A. For a hexagon with $A = L^2$, on the other hand, one obtains $s^2 = 2L^2/3\sqrt{3}$ and $\sigma_A^2 = 1.44\sigma_{coord}^2 L^2$ (where s is the length of a line segment on the boundary of the hexagon, see Fig.2). The issue of adding more vertices while keeping the shape of the polygon is addressed in Sect. 3.6.

The question arises how large the smallest detectable area change is in a SAR image? To address this question, we assume a square grid cell with its vertices on the positions of adjacent displacement vectors and its sides parallel to the x- and y-axes of a Cartesian coordinate system. The cell covers $m \times m$ square-shaped pixels. The minimum possible change is to move one edge point by the side length of one pixel, either in x- or y- direction. This adds the area of a right triangle with legs Δx and $m\Delta x$ ($\Delta y = \Delta x$) and the change of the area is $\Delta A = ½\, m\Delta x^2$, i.e. $100/(2m)$ percent of the original area $(m\Delta x)^2$. Hence the larger the number of pixels in the area, the smaller the detectable relative area change. However, here we assumed that the position error is zero, but we have to consider the uncertainty of the area estimate, which is $\sigma_A^2 = 2\sigma_{coord}^2 m^2 \Delta x^2$ for a square with $L = m\Delta x$. To be sure that a detected area change is real, ΔA needs to be larger than σ_A or $\sigma_{coord} < \frac{1}{2\sqrt{2}}\Delta x$.

2.4 Uncertainties for divergence, shear, vorticity, and total deformation in fixed grids

We consider a grid with displacement or drift velocity vectors on the vertices. For calculating the deformation parameters, we need the velocity gradients u_x, u_y, v_x, v_y, obtained from Eq. (5). Formally, the gradients depend on the area A, positions (x_i, y_i), and velocities (u_i, v_i), see Sect. 2.5. Here we assume that the geo-referencing of the satellite images is accurate. In this case, the positions (x_i, y_i) of vertices and the area of each grid cell are known precisely, which means that $\sigma_{coord} = 0$ and $\sigma_A = 0$. The displacement or velocity vectors, however, have an uncertainty related to the tracking error. With $\partial u_x/\partial u_k = (y_{k+1} - y_{k-1})/(2A^2)$ and again considering that two terms in the sum Eq. (5) include u_i, we obtain:

$$\sigma_{ux}^2 = \frac{\sigma_u^2}{4A^2}\sum_{i=1}^{n}(y_{i+1} - y_{i-1})^2 \tag{13}$$

and analogous equations for the other gradient components. The divergence is $\dot{\boldsymbol{\varepsilon}}_{div} = u_x + v_y$, Eq. (3a), and the corresponding uncertainty is $\sigma_{div} = \sqrt[2]{\sigma_{ux}^2 + \sigma_{vy}^2}$, if u_x and v_y are independent. Throughout this section we assume that $\sigma_U = \sigma_u = \sigma_v$. Hence the error variance for the divergence is

$$\sigma_{div}^2 = \frac{\sigma_U^2}{4A^2}\sum_{i=1}^{n}[(y_{i+1} - y_{i-1})^2 + (x_{i+1} - x_{i-1})^2] \tag{14}$$

Equation (14) resembles the uncertainty for a polygon, Eq. (11). For the vorticity Eq. (3b) one obtains $\sigma_{vrt} = \sqrt[2]{\sigma_{vx}^2 + \sigma_{uy}^2}$ and thus the same expression as for the divergence. The shear rate is given by Eq. (3c). Calculating the derivatives with respect to the velocity gradient components and applying the law of error propagation yields:

$$\sigma_{shr}^2 = \frac{(u_x - v_y)^2}{\dot{\varepsilon}_{shr}^2}\left(\sigma_{ux}^2 + \sigma_{vy}^2\right) + \frac{(u_y + v_x)^2}{\dot{\varepsilon}_{shr}^2}\left(\sigma_{uy}^2 + \sigma_{vx}^2\right) \tag{15}$$

Focusing on the right side of this equation, it is obvious that the sum of variances of the left term is the variance of divergence, the sum in the right term the variance of vorticity. Hence the variances of error are equal for divergence, vorticity and shear.

https://doi.org/10.5194/tc-2020-8
Preprint. Discussion started: 3 February 2020


The Cryosphere Discussions
Open Access
EGU

For the total deformation, Eq. (3d), we need the derivatives $\partial(\dot{\varepsilon}_{tot})/\partial(\dot{\varepsilon}_{shr})$ and $\partial(\dot{\varepsilon}_{tot})/\partial(\dot{\varepsilon}_{div})$ with which we obtain

$$\sigma_{\mathrm{tot}}^2 = \frac{\dot{\varepsilon}_{shr}^2}{\dot{\varepsilon}_{tot}^2}\sigma_{shr}^2 + \frac{\dot{\varepsilon}_{div}^2}{\dot{\varepsilon}_{tot}^2}\sigma_{div}^2 \quad (16)$$

Since the uncertainties for shear and divergence are of equal magnitude, it follows that

$$\sigma_{tot}^2 = \sigma_{shr}^2 = \sigma_{div}^2 = \sigma_{vrt}^2 \quad (17)$$

In the following, we assume that σ_T can be neglected and that the standard deviations for the velocity components *u* and *v* are equal. Using Eq. (14) for a square cell, we obtain for the uncertainty of the divergence:

$$\sigma_{\mathrm{div}}^2 = \frac{\sigma_U^2}{4A^2}(4L^2 + 4L^2) = \frac{2\sigma_d^2}{L^2\Delta T^2} = \frac{4\sigma_{coord}^2 + 2\sigma_{tr}^2}{L^2\Delta T^2} \quad (18)$$

with $A = L^2$, $\sigma_U^2 = \sigma_d^2/\Delta T$, and $\Delta T = t\text{-}t_0$ as above. When the position uncertainty is zero, σ_d depends only on the tracking error (compare to Eqs. (16) and (17) in Lindsay and Stern, 2003).

2.5 Uncertainties of deformation parameters, general case

For an array of buoys, we have to consider errors of the area, the buoy velocity components *u* and *v*, and the coordinates (*x*, *y*) of each buoy position. This is also valid when retrieving deformation from satellite images for which geolocation errors cannot be neglected. A buoy array consists of single buoys arbitrarily positioned over a plane. When connecting all buoy positions with lines, a polygon of area A is formed in which distances between adjacent buoys are usually different. The starting point is Eq. (5). In the following equations summation bounds from $i = 1$ to n are omitted.

For u_x, e. g., we obtain

$$\sigma_{ux}^2 = \sigma_A^2\left(\frac{\partial u_x}{\partial A}\right)^2 + \sigma_u^2\sum\left(\frac{\partial u_x}{\partial u_i}\right)^2 + \sigma_y^2\sum\left(\frac{\partial u_x}{\partial y_i}\right)^2 \quad (19)$$

With $\frac{\partial u_x}{\partial A} = -\frac{1}{2A^2}\sum(u_{i+1}+u_i)(y_{i+1}-y_i)$,

$\frac{\partial u_x}{\partial u_k} = \frac{1}{2A}(y_{k+1} - y_{k-1})$, and $\frac{\partial u_x}{\partial y_k} = -\frac{1}{2A}(u_{k+1} - u_{k-1})$, Eq. (19) reads:

$$\sigma_{ux}^2 = \frac{\sigma_A^2}{4A^4}[\sum(u_{i+1}+u_i)(y_{i+1}-y_i)]^2 + \frac{\sigma_u^2}{4A^2}\sum(y_{i+1}-y_{i-1})^2 + \frac{\sigma_y^2}{4A^2}\sum(u_{i+1}-u_{i-1})^2 \quad (20)$$

The first term on the right side is calculated on line segments connecting adjacent vertices (i+1,j+1), (i, j), the second and third on chords from (i+1, j+1) to (i-1, j-1). Assuming $\sigma_{coord}^2 = \sigma_x^2 = \sigma_y^2$; $\sigma_U^2 = \sigma_u^2 = \sigma_v^2$ (the latter follows from $\sigma_T^2/\Delta T^2 \approx 0$) one obtains for the divergence:

$$\sigma_{div}^2 = \frac{\sigma_A^2}{4A^4}\{[\sum(u_{i+1}+u_i)(y_{i+1}-y_i)]^2 + [\sum(v_{i+1}+v_i)(x_{i+1}-x_i)]^2\}$$
$$+\frac{\sigma_U^2}{4A^2}[\sum(x_{i+1}-x_{i-1})^2 + \sum(y_{i+1}-y_{i-1})^2] + \frac{\sigma_{coord}^2}{4A^2}[\sum(u_{i+1}-u_{i-1})^2 + \sum(v_{i+1}-v_{i-1})^2] \quad (21)$$

https://doi.org/10.5194/tc-2020-8
Preprint. Discussion started: 3 February 2020

where the first term can be written as $\frac{\sigma_A^2(u_x^2+v_y^2)}{A^2}$, considering Eq. (5), and the second term is $\frac{\sigma_U^2\sigma_A^2}{A^2\sigma_{coord}^2}$, from Eq. (12). For the vorticity, only the first term is different:

$$\sigma_{vrt}^2 = \frac{\sigma_A^2(u_y^2+v_x^2)}{A^2} + \frac{\sigma_U^2}{4A^2}\left[\sum(x_{i+1}-x_{i-1})^2 + \sum(y_{i+1}-y_{i-1})^2\right] + \frac{\sigma_{coord}^2}{4A^2}\left[\sum(u_{i+1}-u_{i-1})^2 + \sum(v_{i+1}-v_{i-1})^2\right] \quad (22)$$

The first term in Eqs. (21) and (22) considers that the relative error variance of the area affects the magnitude of the average velocity gradients. The second term is the variance of divergence/vorticity of the velocity field in a fixed grid where positions of vertices are known precisely, Eq. (14). The last term takes into account the effect of uncertainties in the positions of buoys in the field of velocity vectors. The velocity is usually determined from buoy positions (or positions of detectable ice structures in SAR images) separated by a time interval $\Delta T=T_{i+1}-T_i$. However, within ΔT also the buoy array (or a grid cell in the Lagrangian approach) changes its area and shape. Hence an optimal approach would be to determine the average velocity from positions at T_{i-1}, T_i, and T_{i+1} and link it with the geometric properties of the buoy array (grid cell) at time T_i. For the shear one obtains

$$\sigma_{shr}^2 = \frac{(u_x-v_y)^2}{\varepsilon_{shr}^2}\left(\sigma_{ux}^2+\sigma_{vy}^2\right) + \frac{(u_y+v_x)^2}{\varepsilon_{shr}^2}\left(\sigma_{uy}^2+\sigma_{vx}^2\right) \quad (23)$$

where σ_{ux}, σ_{uy}, σ_{vx}, σ_{vy} are calculated using Eq. (20) and analogous expressions. For the total deformation

$$\sigma_{tot}^2 = \frac{\varepsilon_{shr}^2}{\varepsilon_{tot}^2}\sigma_{shr}^2 + \frac{\varepsilon_{div}^2}{\varepsilon_{tot}^2}\sigma_{div}^2 \quad (24)$$

Hence, the uncertainties of divergence, vorticity, shear, and total deformation differ from one another. In practical applications, they can be evaluated numerically. This requires the knowledge of uncertainties σ_{coord} for buoys and σ_{coord}, σ_{tr} for satellite images.

3 Discussion

Eqs. (21) to (24) provided above indicate that statistical uncertainties are not only influenced by geolocation and tracking errors but also depend on the shape and size of grid cells and buoy arrays. In the following discussion we consider magnitudes of geolocation and tracking errors reported in the literature and selected squares and triangles as examples for grid cells in SAR images (Lindsay, 2002; Bouillon and Rampal, 2015) and for splitting large buoy arrays into smaller units (Hutchings et al., 2012; Itkin et al., 2017). The effect of combining several cells is investigated. Finally, we focus on the range of validity of the equations derived in Sect. 2, and alternative methods of analysis.

3.1 Typical uncertainties of deformation parameters

The statistical uncertainties have to be related to the typical magnitudes of the deformation parameters. According to Leppäranta (2011, p.70) the total deformation of drifting ice typically varies between around 90% d^{-1} in the marginal ice zone to 0.9% d^{-1} in the central Arctic. For the vorticity, magnitudes up to 9% d^{-1} = ½ (0.09) revolutions d^{-1} = 16.2° d^{-1} were observed. Hutchings et al. (2012, Figs. 4 and 7) analyzed displacements of an array of 24 buoys deployed in the Weddell Sea on continuous first- and second-year ice with concentrations above 90 percent. For the divergence, they found most values between -90% d^{-1} and 90% d^{-1} at a spatial scale of 10 km, at 60 km scale mainly between ±25% d^{-1}, and up to 35% d^{-1} for the

https://doi.org/10.5194/tc-2020-8
Preprint. Discussion started: 3 February 2020

shear. Itkin et al. (2017b) observed single events of strong divergence and shear of up to 200% d^{-1} from buoys in an area north of Svalbard, but most values for divergence ranged between roughly ±10% d^{-1}, for shear between 0 and 10% d^{-1}. Based on merged velocity measurements from buoys and different satellite sensors, Lindsay (2002) provided a table for monthly averaged values of divergence (-0.6 to 0.5% d^{-1}), shear (0.9 to 4% d^{-1}), and vorticity (-2.3 to 3.2% d^{-1}) from the Beaufort Sea. Stern and Moritz (2002, Fig. 4) used SAR images and found decreasing magnitudes for the divergence for increasing spatial scales from 50×50 km to 200×200 km in the Beaufort Sea. Magnitudes were largest between August and February with minima/maxima between -5% d^{-1} and 5% d^{-1}. Note that the uncertainties resulting from the equations given in the subsections below have to be multiplied by 100 to obtain a value in percent per time unit.

3.2 Uncertainties for areas of simple geometric shape

In general, the uncertainty of the deformation parameters depends on the ratio σ_{coord}^2/A^2 (since σ_A and σ_U are functions of σ_{coord}), hence for given geolocation and tracking errors it decreases with increasing area. The first term in Eqs. (21) and (22) is smallest if, for a given area, σ_A is at a minimum. For an arbitrary triangle with sides a, b, c, the uncertainty σ_A^2 is $0.25\sigma_{coord}^2(a^2+b^2+c^2)$ (see Fig. 2). Of all triangles with the same base and the same area A, the equal-sided triangle with $a = b = c$ has the smallest perimeter and hence the lowest uncertainty, which is $\sigma_A^2 = \sqrt{3}\sigma_{coord}^2 = 1.73\sigma_{coord}^2$ for a unit area. (This follows from the equations for the area of the equal-sided triangle which is $A = \frac{\sqrt{3}}{4}a^2$ and for the uncertainty $\sigma_A^2 = \frac{3a^2}{4}\sigma_{coord}^2$ if $A = 1$). For the regular hexagon, which is composed of six equal-sided triangles, one obtains $\sigma_A^2 = \frac{5}{2\sqrt{3}}\sigma_{coord}^2 = 1.44\sigma_{coord}^2$ (Fig. 2). In case of rectangles and rhombi, squares have the smallest perimeter (see Fig. 2). In both cases the uncertainty is $\sigma_A^2 = 2\sigma_{coord}^2$ for a unit area, hence larger than for the equal-sided triangle.

3.3 Uncertainties in time

The accuracy of time readings for the acquisitions of satellite images is on the order of sub-seconds. The product of sea ice drift velocity and uncertainty of time reading appears on the right-hand side of Eq. 6: $2\sigma_{coord}^2 + \sigma_{tr}^2 + u^2\sigma_{\Delta T}^2$. Average sea ice drift velocities range mostly from 0 to 0.35 m/s (Rampal et al., 2009). Kræmer et al. (2015) determined instantaneous line-of-sight ice drift velocities, using Doppler frequency measurements from SAR, and found values as large as 0.4-0.6 m/s. If we assume a maximum value of u = 1 m/s and a maximum uncertainty of time readings of 1 millisecond, the term $u^2\sigma_{\Delta T}^2$ on the right side of Eq. (6) is 10^{-6} m^2 at the most. It can be neglected compared to the typical values of terms σ_x^2, σ_y^2 and $\sigma_{tr_x}^2$, $\sigma_{tr_y}^2$ in Eq. (6) (see Sect. 3.4 for a discussion of the effect of position and tracking errors). The uncertainty $\sigma_{\Delta T}$ of the GPS time (used both for buoys and satellites such as Sentinel-1) is given as better than one millisecond (see, e.g. websites [1] and [2]). Similar considerations apply to Eq. 8. Hence, in Eqs. (21) and (22) we have $\sigma_U^2 = (2\sigma_{coord}^2 + \sigma_{tr}^2)/\Delta T^2$ both for velocity (displacement) retrievals from satellite image pairs and buoy arrays. For a given position error, the second term in Eq. (21) decreases with increasing time interval ΔT and area A. The third term is solely dependent on the coordinate uncertainty σ_{coord}.

Another issue that has to be considered is the time synchronization between individual buoys in an array. Differences of a few seconds may be possible in practice. In the following discussion we assume that position data of all buoys are exactly synchronized but also discuss an example for which this was not the case.

3.4 Deformation retrievals from square grid cells in SAR images

Here we first focus on the retrieval of deformation parameters from SAR images. If a square of side length L, with sides parallel to the x- and y-axes, is positioned in a spatially varying velocity field as shown in Fig. 3, the uncertainty of the divergence is:

https://doi.org/10.5194/tc-2020-8
Preprint. Discussion started: 3 February 2020


The Cryosphere Discussions
Open Access
EGU

$$\sigma_{div}^2 = \frac{3\sigma_{coord}^2}{L^2}\left(u_x^2 + v_y^2\right) + \frac{\sigma_{coord}^2}{L^2}\left(u_y^2 + v_x^2\right) + \frac{4\sigma_{coord}^2}{\Delta T^2 L^2} + \frac{2\sigma_{tr}^2}{\Delta T^2 L^2} \quad (25)$$

This follows from Eq. (21) with the velocities given in Fig. 3 at the edges 1-4 of the square. The uncertainty of the vorticity is from Eq. (22)

$$\sigma_{vrt}^2 = \frac{3\sigma_{coord}^2}{L^2}\left(u_y^2 + v_x^2\right) + \frac{\sigma_{coord}^2}{L^2}\left(u_x^2 + v_y^2\right) + \frac{4\sigma_{coord}^2}{\Delta T^2 L^2} + \frac{2\sigma_{tr}^2}{\Delta T^2 L^2} \quad (26)$$

Uncertainties of shear and total deformation can be calculated using Eqs. (23) and (24). The second term in Eq. (25) and first term in Eq. (26) indicates that the uncertainties of divergence and vorticity are affected by contributions from pure shear. The third and fourth term of Eq. (25) are independent of the velocity gradients and are only a function of position and tracking error, time interval between position measurements, and size of the square. The fourth term is equal to Eq. (17) in Lindsay and Stern (2003). When ice drift is retrieved from SAR images, the contribution of those terms that depend on σ_{coord}/L can usually be neglected. For Envisat ASAR stripmap and wide-swath mode images (IM and WSM), e.g., Small et al. (2005) reported differences between measured positions of reflectors and their positions in the SAR image of 1.63±0.82 m in azimuth (considering bi-static correction) and 2.02±0.51 m in slant range for normal imaging mode in single-look complex format. Ground range products require the transformation from slant- to ground-range as an additional step. When judging the effect of position errors on the uncertainty of divergence and vorticity, the systematic bias (mean error) of positions affects all vertices of a grid cell in the same way, hence only the standard deviation σ has to be considered. Here we use a value of 1 m as a conservative estimate of the azimuth and ground-range position uncertainty for IM. For ground-range WSM images, the accuracy of positioning was better than one pixel. If we assume that the ratio σ[m]/σ[pixel] is approximately the same for IM and WSM, the uncertainty for the latter is about 7 m at maximum. In the study of Hollands and Dierking (2011), e.g., resolution pyramids and cascades are used for retrieving sea ice displacements from Envisat ASAR IM and WSM data. For the level of highest spatial resolution the side lengths of the grid cells (distance between adjacent displacement vectors) was 300 m for IM and 1500 m for WSM. Hence, the corresponding ratios $\sigma_{coord}{}^2/L^2$ are on the order of $1^2/300^2 \approx 10^{-5}$ and $7^2/1200^2 \approx 3.4 \times 10^{-5}$, respectively. For modern SAR systems such as TerraSAR-X and Sentinel-1, the positioning accuracy is even better than for Envisat (e.g. Schubert et al., 2008; Schubert et al., 2017).

The third and fourth term in Eqs. (25) and (26) can be directly computed from position and tracking error, the time interval ΔT between image acquisitions, and the grid cell size. The first and second term of Eqs. (25) and (26) include expressions $(u_x^2 + v_y^2)$ and $(u_y + v_x)^2$. If we assume that the divergence, Eq. 3a, is $u_x + v_y = 1$ d^{-1}, with $v_y = 0$ and a maximum possible ratio $\sigma_{coord}{}^2/L^2 = 10^{-4}$, the magnitude of the first term in Eq. (25) is 0.0003 d^{-2} and the second term in Eq. (26) is 0.0001 d^{-2}. A value of 1d^{-1} can be regarded as an extremely large divergence rate rarely observed in reality (see Sect. 3.1). Maximum vorticities $(v_x - u_y)$ are about 0.1 d^{-1} at most. For our example, the third term $(4/\Delta T^2) \times (\sigma_{coord}{}^2/L^2)$ in Eqs. (25) and (26) ranges between 0.00004 d^{-2} and 0.23 d^{-2} for ΔT between 3 days and one hour. The ratio between the fourth and the third term is $\sigma_{tr}{}^2/2\sigma_{coord}{}^2$. Since the position uncertainty is usually much smaller than the side length of a pixel, and the tracking uncertainty is of similar magnitude or larger, the fourth term is dominant in many cases.

In their study mentioned above, Hollands and Dierking (2011) found tracking errors between 0.8 and 1.6 pixels (their Tables 3 and 4, standard deviations), which corresponded to 20 - 40 m for IM and 120 – 240 m for WSM. With σ_{coord} = 1 m for IM and 7 m for WSM, the ratios between fourth and third term are hence 200 – 800 for IM and 148 – 588 for WSM. In this case the first three terms can be neglected compared to the fourth. With a grid cell size of L = 300 m (IM) and 1200 m (WS), and time differences ranging from 1.2 to 5.8 days for IM image pairs and from 2 to 6 days for WSM image pairs, the uncertainties σ_{div} and σ_{vrt} were between 2.6% / ΔT d^{-1} and 14 % / ΔT d^{-1} for IM and 2.8 % / ΔT d^{-1} and 9 % / ΔT d^{-1} for WSM (calculated for each image pair listed in Table 1 of Hollands and Dierking (2011), with the corresponding tracking errors from

https://doi.org/10.5194/tc-2020-8
Preprint. Discussion started: 3 February 2020

their Tables 3 and 4). Comparing these values to the typical magnitudes of divergence and vorticity given above, the respective uncertainties are too large in areas of weaker deformation. Lindsay and Stern (2003), e.g., calculated deformation parameters for the RGPS initial velocity grid (L=10 km), and a time interval ΔT of 3 days. They found a tracking error of 100 m for Radarsat ScanSAR images (pixel size 100 m), with $\sigma_{tr}^2/2\sigma_{coord}^2$ approximately equal to $100^2/(2\times5^2) = 200$. From the fourth term we get uncertainties for divergence and vorticity of 0.5% d^{-1}. At first sight, larger time intervals and grid cells seem to be advantageous. However, larger time intervals may cause problems in the retrieval of the ice drift field, since ice structures, which serve as reference for the retrieval, may change or even vanish with time. Deformation parameters are inversely proportional to the size of the grid cell over which they are estimated, see Eq. (5). This means that for smaller scales, the uncertainty of the estimates increases. If we assume that an uncertainty of 1% d^{-1} is still acceptable for divergence and vorticity in many cases, then the fourth term of Eqs. (25) and (26) tells us that the ratio between tracking uncertainty and grid cell size, σ_{tr}/L, should satisfy $\sigma_{tr}/L \leq 0.01\,[d^{-1}] \times \Delta T[d]/\sqrt{2} \cong 0.007[d^{-1}] \times \Delta T[d]$. For ΔT = 1 d, this means a grid cell length of roughly 150 × σ_{tr} (uncertainty 1% d^{-1}) or larger (uncertainty < 1% d^{-1}).

3.5 Deformation retrievals from triangular grid cells or buoy arrays

Triangles are used for calculations of deformation parameters in SAR images (e.g. Bouillon and Rampal, 2015; Griebel and Dierking, 2018) and form the smallest units of buoy arrays (e.g. Hutchings et al., 2011; Hutchings et al., 2012). Using the same approach as for the square above, we obtain for a triangle with its base a parallel to the x-axis (Fig. 4):

$$\sigma_{div}^2 = \frac{\sigma_{coord}^2(a^2+b^2+c^2)}{h_a^2 a^2}\left(u_x^2+v_y^2\right) + \frac{(2\sigma_{coord}^2+\sigma_{tr}^2)(a^2+b^2+c^2)}{\Delta T^2 h_a^2 a^2}$$

$$+\frac{2\sigma_{coord}^2}{h_a^2 a^2}\left[(u_x^2+v_x^2)(a^2+a_1^2-aa_1)+\left(u_y^2+v_y^2\right)h_a^2+\left(u_xu_y+v_xv_y\right)(2a_1-a)h_a\right] \quad (27)$$

For the vorticity, the sum ($u_x^2 + v_y^2$) in the first term has to be replaced by ($u_y^2 + v_x^2$). Equation (27), which is shown here for an acute triangle (all internal angles <90°), is also valid for an obtuse triangle (one internal angle >90°) setting a_1 negative and a_2 to zero. For a right triangle with $b = a$, $c = \sqrt{2}a$, $h_a = a$, and $a_1 = a$, Eq. (27) yields

$$\sigma_{div}^2 = \frac{6\sigma_{coord}^2}{a^2}\left(u_x^2+v_y^2\right)+\frac{2\sigma_{coord}^2}{a^2}\left(u_y^2+v_x^2+\left(u_xu_y+v_xv_y\right)\right)+\frac{8\sigma_{coord}^2}{\Delta T^2 a^2}+\frac{4\sigma_{tr}^2}{\Delta T^2 a^2} \quad (28a)$$

However, if the right angle is placed at the left side of the triangle, i.e. $c = a$, $b = \sqrt{2}a$, $h_a = a$, and $a_1 = 0$, the resulting equation changes to:

$$\sigma_{div}^2 = \frac{6\sigma_{coord}^2}{a^2}\left(u_x^2+v_y^2\right)+\frac{2\sigma_{coord}^2}{a^2}\left[u_y^2+v_x^2-\left(u_xu_y+v_xv_y\right)\right]+\frac{8\sigma_{coord}^2}{\Delta T^2 a^2}+\frac{4\sigma_{tr}^2}{\Delta T^2 a^2} \quad (28b)$$

Considering the conclusions above, drawn for a grid of squares, the contributions of terms 1-3 of Eqs. (28a) and (28b) can be neglected in many cases when using SAR for the retrieval of drift vectors. When comparing the third and fourth terms of Eqs. (28) and (25) one finds that the squared uncertainty of a right triangle is two times the squared uncertainty of a square for $a = L$ and identical σ_{coord}, σ_{tr}, and ΔT, which can be attributed to the reduced coverage of the triangle over the varying velocity field. For an uncertainty of 1% d^{-1}, we obtain a value of $\leq 0.005[d^{-1}]\times\Delta T[d]$ for the ratio σ_{tr}/a, corresponding to a base length a of 200 × σ_{tr} if ΔT = 1d.

https://doi.org/10.5194/tc-2020-8
Preprint. Discussion started: 3 February 2020


The Cryosphere Discussions

The uncertainty of the equal-sided triangle ($c = b = a$, $h_a^2 = 3a^2/4$, and $a_1 = a/2$) is

$$\sigma_{div}^2 = \frac{6\sigma_{coord}^2}{a^2}\left(u_x^2 + v_y^2\right) + \frac{2\sigma_{coord}^2}{a^2}\left(u_y^2 + v_x^2\right) + \frac{8\sigma_{coord}^2}{\Delta T^2 a^2} + \frac{4\sigma_{tr}^2}{\Delta T^2 a^2} \quad (29)$$

Note that compared to a square of length L, the area of an equal-sided triangle with base L is $0.433A_{square}$. The area of an arbitrary triangle with constant base increases when changing its shape from the equal-sided to the right triangle.

For buoys, the tracking error is zero. Itkin et al. (2017) quoted 25 m as geolocation accuracy for stationary buoys but used 50 m to account for effects of buoy drift. One of us (Hutchings) analyzed the position errors of GPS receivers in the Fairbanks (Alaska) region. The errors were normally distributed for position data collected at the same location for several days. The relative position error between pairs of GPS receivers, which has to be used for deformation calculations, was 2 m over distances of 1-10 km. Reported time intervals between acquisitions of buoy positions range from 10 seconds to 3 hours (Hutchings, 2012; Itkin et al., 2017) with uncertainties in time less then milliseconds (see above). Hutchings at al. (2012), however, mention also a time error of 30 seconds, which was due to the acquisition times of the buoys not being exactly time coincident. In such exceptional case, the second term on the right-hand side of Eq. (8) cannot be neglected if the position uncertainty is small. If the ice drifts in x-direction (i.e. $v = 0$), the right-hand side of Eq. (8) reads $(2\sigma_{coord}^2 + u^2\sigma_{\Delta T}^2) / \Delta T^2$ ($\sigma_{tr} = 0$ for buoys). When the magnitude of the second term is 1% of $2\sigma_{coord}^2$ or less, hence negligible, the velocity u must be equal or smaller than 424 m/h if we assume that $\sigma_{coord} = 25$ m and $\sigma_{\Delta T} = 30$ s. If $\sigma_{coord} = 2$ m, the result is $u = 34$ m/h. The speed of sea ice drift ranges mainly between 0 and 1.5 km/h, with possible maximum around 3.6 km/h (see Sect. 3.3) which means that the term $u^2\sigma_{\Delta T}^2$ has to be taken into account in most cases. Conversely, we may ask how large the acceptable maximum uncertainty is so that the second term is negligible (i.e. < 1% compared to the first term). With u = 3.6 km/h = 1 m/s and σ_{coord} = 2 m one obtains $\sigma_{\Delta T} = 0.3$ s, and for $\sigma_{coord} = 25$ m it is $\sigma_{\Delta T} = 3.5$ s.

In the following examples we assume that the temporal sampling error can be neglected. For judging the uncertainty of deformation rates, the time interval ΔT is set to the temporal sampling rate of buoy positions. As an example, we use right triangles, Eqs. (28a) and (28b), and equal-sided triangles, Eq. (29). Here, the fourth term on the left side, containing the tracking error, is zero. Itkin et al. (2017) analyzed deformation for constellations of three buoys and reported divergence values mostly in the range ±10% d^{-1}, which is about ±0.4% h^{-1}=±0.004h^{-1}. The smallest distance between buoys was 2 km, the largest 70 km. If, e.g., $u_x = \pm 0.004$ h^{-1} and $v_y = u_y = v_x = 0$, the second term in Eqs. (28a), (28b) and (29) is zero. For temporal sampling intervals of $\Delta T = 1$h and $\Delta T = 3$h, as given in Itkin et al. (2017), the first term, which is 0.00006 σ_{coord}^2/a^2 h^{-2} for Eqs. (28a) and (28b), and $0.0001\sigma_{coord}^2/a^2$ h^{-2} for Eq. (29), can be neglected compared to the third term $(8/\Delta T^2) \times (\sigma_{coord}^2/a^2)$. From the latter, the uncertainty of the divergence is hence $\sigma_{div} = 71/a$ h^{-1} for $\Delta T = 1$h and $24/a$ h^{-1} for $\Delta T = 3$ h, where $\sigma_{coord} = 25$ m and the value for base a has to be given in meters. If we accept an uncertainty of $\sigma_{div} \leq 0.0004h^{-1}$ (which is 10% or less relative to the majority of the measured deformation rates), base a of the triangle has to be larger than 177 km for $\Delta T = 1$h and 59 km for $\Delta T = 3$h. If one calculates the divergence using only the position change after 24 hours, the required base is $2.96/a$ h^{-1}, and for $\sigma_{div} = 0.0004h^{-1}$ one obtains a =7.4km. Hence, by choosing a larger time interval, acceptable uncertainties can be obtained over smaller spatial scales. If positions acquired at shorter time intervals are available, they can be used for controlling the temporal evolution of the ice drift. Using $\sigma_{coord} = 2$ m instead of 25 m in the example given above, we obtain $\sigma_{div} = 5.7/a$ h^{-1} for $\Delta T = 1$h, i.e. a base length of 14 km for a single measurement with $\sigma_{div} = 0.0004$ h^{-1}, and 0.6 km for one measurement with $\Delta T = 24$ hours.

Since the area and shape of the triangle change under the action of continuous stress, the uncertainty does not simply decrease by a factor of $1/\sqrt{n}$, i.e. with the number n of buoy position readings. If we assume that the three-buoy array keeps the shape of an equal-sided triangle for 24 hours, with an increase in side length from a_0 to $1.1a_0$ (i.e. the area of the triangle

https://doi.org/10.5194/tc-2020-8
Preprint. Discussion started: 3 February 2020


The Cryosphere Discussions
Open Access
EGU

increases by a factor of 1.05), the uncertainty of the last single measurement at the end of the 24 hour period is lower by a factor of 1/1.1=0.91, Eq. (29, third term). Here it is assumed that the divergence is constant, the ratio u_x/v_y is fixed by the ratio between base a and height h_a of the triangle, and the vorticity is zero, i.e. $u_y=v_x=0$. As mentioned above, the position error may be as small as 2 m.

3.6 Combination of grid cells or buoys

The combination of grid cells or several buoys is one possibility to lower the uncertainty of the area σ_A,. In general, the uncertainty of deformation rates is reduced when they are evaluated over a larger area, as can be deduced from the equations provided in Sects. 2.4 and 2.5. However, the uncertainty of the area, σ_A, appears explicitly only in the equations derived for the general case, Sect. 2.5. In Sects. 3.4 and 3.5 we showed that the terms including σ_A can be neglected since velocity gradients observed for sea ice are usually small. Since, on the other hand, the change of the area inside a buoy array or of a grid cell can also be used to quantify deformation (Lindsay and Stern, 2003), it is worthwhile to have a closer look at the effect of combining several grid cells or buoys.

Because buoy arrays rarely reveal simple shapes such as squares or right triangles, the uncertainties have to be calculated numerically. Hutchings et al. (2012), e.g., used 22 buoys, which they split into arrays of approximately equilateral triangles, but also into arrays of six, nine, and twelve buoys. Here we discuss combinations of squares and triangles.

First we investigate the effect of splitting a square or a right triangle into smaller units. We start with a square window covering $N \times N$ cells, i.e. we have $4N$ displacement vectors around it. Let L' be the length of each side of the big square (Fig. 5). Because of the enclosed grid cells we can divide each side of the square window into N segments of equal length. If $N = 2$ then each side of the window is 2 segments of length $L'/2$, and correspondingly for $N > 2$ it is L'/N. The term $\Sigma(x_{i+1} - x_{i-1})^2$ is zero if both x_{i+1} and x_{i-1} are located on the vertical sides of the window. On the top and bottom sides parallel to the x-axis, $N-1$ terms in the summation contribute $(2L'/N)^2$ for each side (indicated by green bars in Fig. 3). In addition, each corner contributes $(L'/N)^2$ (blue bars). The total contribution is hence $2(N-1)(2L'/N)^2 + 4(L'/N)^2 = 4(2N-1)(L'/N)^2$. The term $\Sigma\ (y_{i+1} - y_{i-1})^2$ contributes the same amount. Hence application of Eq. (12) yields:

$$\sigma_A^2 = \sigma_{coord}^2\ (4N - 2)\ (L'/N)^2 \qquad (30a)$$

Since each side of the square is divided into N segments, the total number of points defining the boundary is $n = 4N$. With $L = L'/N$, we can rewrite Eq. (30) as $\sigma_A^2 = \sigma_{coord}^2(n-2)L^2$ which is Eq. (16) in Lindsay and Stern (2003). However, the notation in Eq. (30), using N and L' instead of n and L, is preferable because it explicitly shows that σ_A^2 decreases as N increases for a fixed L'.

For a right triangle, we have only two contributions from the corners instead of four as for the square (Fig. 5). In x-direction, e. g., the term $x_{i+4} - x_{i+2}$ is zero. Hence the total contribution in x- and y-direction is $4(N-1)(2L'/N)^2 + 4(L'/N)^2$ or

$$\sigma_A^2 = \sigma_{coord}^2\ (4N - 3)\ (L'/N)^2 \qquad (30b)$$

Note that σ_A^2 for the right triangle is $\sigma_{coord}^2 L'^2$ for $N = 1$, $1.25\sigma_{coord}^2 L'^2$ for $N = 2$, $\sigma_{coord}^2 L'^2$ for $N = 3$, and $0.8125\sigma_{coord}^2 L'^2$ for $N = 4$, i.e. for $N = 2$ the uncertainty increases, $N = 3$ and $N = 1$ reveal the same uncertainty, and first with $N = 4$, the uncertainty can be reduced.

In SAR applications, the question is whether it is preferable to use, e.g., the smallest possible ("elementary") square cell (determined by the resolution of the ice drift field) with four drift vectors at the edges, or to combine adjacent cells. Formally, the uncertainty in area for the elementary cell is $2\sigma_{coord}^2 L^2$, and for a cell with side length $L' = N \times L$, covering $N \times 4$ drift vectors, Eq. (30a) yields $\sigma_A^2 = \sigma_{coord}^2(4N-2)L^2$. Hence the uncertainty of the area increases when elementary cells are combined. However, since also the cell area increases by a factor of N^2, the single terms in Eqs. (13) – (22) that include the

https://doi.org/10.5194/tc-2020-8
Preprint. Discussion started: 3 February 2020

factor A^{-2} decrease. The effect of local variations of the drift field on the deformation rate can be considered in more detail when more vertices or buoys are included in the calculations.

For buoy arrays it may be of advantage to use a larger number of buoys along the outline of a polygon. Here we study the example of an isosceles triangle with two sides of equal length (Fig. 6), which, e.g., comes closest to the array / subarrays used by Hutchings et al. (2012). The term $\Sigma(x_{i+1} - x_{i-1})^2$ of Eq. (12) results in $(6N\text{-}4.5)(L'/N)^2$, for the term $\Sigma\,(y_{i+1} - y_{i-1})^2$ we obtain $(8N\text{-}6)(h/N)^2$.The areal uncertainty is hence:

$$\sigma_A^2 = (\sigma_{coord}^2/2)\,[(3N - 2.25)\,(L'/N)^2 + (4N\text{-}3)(h/N)^2] \quad (31)$$

Compared to an array consisting of three buoys at the edges of the triangle, the uncertainty can be reduced for $N \geq 4$, i.e. at least 12 buoys are required along the outline of the triangle.

If the shape of an array with many buoys approximately approaches the shape of a circle with radius r, and if the sum of two line segments s connecting vertices with summation index i+1 and i differs only slightly compared to the chord length s_c between vertices i+1 to i-1, the uncertainty of the area can be estimated as follows. We require that $s_c^2 \approx (2s)^2$. According to Eq. (12) the uncertainty in area is

$$\sigma_A^2 = \frac{\sigma_{coord}^2}{4}\sum_{i=1}^{n} s_{ci}^2 = \frac{\sigma_{coord}^2}{4} n s_c^2 \approx \frac{\sigma_{coord}^2}{4} n 4s^2 \approx \sigma_{coord}^2\, n \left(r\,\frac{2\pi}{n}\right)^2 = \frac{4\sigma_{coord}^2}{n}\pi^2 r^2 \quad (32)$$

in agreement with Jansson and Persson (2014, equation 29). Here we use the relationship $s = 2\pi r/n$ and take into account that both the even chords (i-1, i+1) with i=1,3,5,… and the odd chords with i=2,4,6,… each approximate the total perimeter of the circle (see e.g. Fig. 2, hexagon). To calculate the number of chords that is required to fulfill Eq. (32), we demand that $n's_c\,(1+e) = 2\pi r$, with $n' = n/2$, and e the error. With $s_c/r = 2\sin(\pi/n')$ the condition is $\sin(\pi/n')(1+e) = \pi/n'$. If n'=10 (i.e. a circled-shaped array with 20 buoys), e is < 0.017.

3.7 Validity

It has to be kept in mind that the fundamental Eqs. (1), (2), (4) and (5) that we used for estimating the statistical uncertainties in the retrieval of deformation parameters are based on simplifying assumptions. Hence it is necessary to consider their range of validity when applying them.

3.7.1 Truncation error

The right-hand side of Eq. (5) for estimating u_x is based on the trapezoid rule applied to the contour integral on the left side. The trapezoid rule is exact if u is linear in x and y; otherwise, the non-linear part of u gives rise to a truncation error. Define segment k of the contour integral to be the straight line from (x_k, y_k) to (x_{k+1}, y_{k+1}), and define $\Delta x_k = x_{k+1} - x_k$ and $\Delta y_k = y_{k+1} - y_k$. Then segment k of the contour integral $\oint u dy$ is estimated by $\frac{1}{2}(u_{k+1} + u_k)\Delta y_k$, as in Eq. (5), and the associated error is:

$$e_k = -\frac{1}{12}\left(u_{xx}\Delta x_k^2 + 2u_{xy}\Delta x_k \Delta y_k + u_{yy}\Delta y_k^2\right)\Delta y_k \quad (33)$$

where the partial derivatives are evaluated at some point on segment k. As can be seen, if u is linear in x and y on segment k then $e_k = 0$. Similar error expressions apply to the estimates of the other velocity derivatives.

https://doi.org/10.5194/tc-2020-8
Preprint. Discussion started: 3 February 2020

3.7.2 Spatial resolution

Equation (5) provides an area-averaged estimate of u_x. The question arises as to whether the spatial resolution (i.e. the area) is small enough to capture the spatial variability in $u(x, y)$. One way to answer this question is to sub-divide the region into smaller pieces and repeat the calculation of u_x for each piece. If the variability of u_x from piece to piece is large then the sub-division of the original area was necessary; otherwise, it was not. In practice, sub-dividing a region means adding new data points, which is not always possible, unless the original region is purposely chosen to consist of the union of several smaller pieces. An alternative method for determining whether the spatial resolution is adequate is given at the end of Sect. 3.8 below.

3.7.3 Temporal sampling

What temporal sampling is necessary to resolve changes in the sea-ice velocity field? The velocity may be decomposed into a mean field and a fluctuating part (Thorndike, 1986). Rampal et al. (2009) showed that the variance of the fluctuating part has two regimes separated by a time scale of ~1.5 days. Since buoys deployed on sea ice report their positions every few hours or less, their sampling frequency is sufficient to resolve the velocity and its fluctuations. The revisit time of modern satellite constellations such as Sentinel-1 is less than a day at the high latitudes of the poles but older systems with three-day sampling may have missed some of the deformation caused by spatial variations in those fluctuations.

3.7.4 Correlation of errors

We have assumed that different error sources are uncorrelated and hence we have ignored the second term on the right-hand side of Eq. (2). While it is often true that spatial errors are uncorrelated with temporal errors, it may not always be the case that spatial errors are uncorrelated with each other. For example, for the distance $d = \sqrt[2]{(x' - x)^2 + (y' - y)^2}$ between two points (x', y') and (x, y), the full error variance of d is given by:

$$\sigma_d^2 = \left(\frac{\partial d}{\partial x'}\right)^2 \sigma_{x'}^2 + \left(\frac{\partial d}{\partial x}\right)^2 \sigma_x^2 + \left(\frac{\partial d}{\partial y'}\right)^2 \sigma_{y'}^2 + \left(\frac{\partial d}{\partial y}\right)^2 \sigma_y^2 + 2\left(\frac{\partial d}{\partial x'}\right)\left(\frac{\partial d}{\partial x}\right)\sigma_{x'x}$$
$$+2\left(\frac{\partial d}{\partial y'}\right)\left(\frac{\partial d}{\partial y}\right)\sigma_{y'y} + 2\left(\frac{\partial d}{\partial x'}\right)\left(\frac{\partial d}{\partial y'}\right)\sigma_{x'y'} + 2\left(\frac{\partial d}{\partial x}\right)\left(\frac{\partial d}{\partial y}\right)\sigma_{xy} + 2\left(\frac{\partial d}{\partial x'}\right)\left(\frac{\partial d}{\partial y}\right)\sigma_{x'y} + 2\left(\frac{\partial d}{\partial x}\right)\left(\frac{\partial d}{\partial y'}\right)\sigma_{xy'} \quad (34)$$

If the coordinate uncertainties are all equal ($\sigma_x = \sigma_y = \sigma_{x'} = \sigma_{y'} = \sigma_{coord}$), and the same is valid for the covariances with $\sigma_{xy} = \sigma_{x'y'} = \sigma_{x'y} = \sigma_{xy'} = \sigma_{y'y} = \sigma_{x'x}$ = c, then we obtain $\sigma_d^2 = 2\sigma_{coord}^2 - 2c$. Since the correlation between, e.g., x and y (and correspondingly for all combinations above) is $\rho = \sigma_{xy} / (\sigma_x \sigma_y) = c / \sigma_{coord}^2$ we obtain $\sigma_d^2 = 2\sigma_{coord}^2 (1 - \rho)$. In this case, a positive correlation serves to reduce σ_d^2 while a negative correlation serves to increase it. Since position errors are more likely to be positively correlated (due to systemic bias), ignoring the correlation terms is actually a conservative approach to error estimation.

3.7.5 Velocity discontinuities

When calculating uncertainties of deformation parameters, it is implicitly assumed that the sea-ice velocity does not have discontinuities within the polygon in which the deformation is being estimated. This is because we use Eq. (5), which is based on Green's theorem. Numerous observations of the sea-ice velocity field show narrow shear zones or "linear kinematic features" (e.g. Kwok, 2003; Marsan et al., 2004; Kwok, 2006) across which the velocity jumps abruptly, as a result of stresses in the ice that create leads and ridges. Some researchers, e.g. Griebel and Dierking (2017) have proposed methods to detect and isolate these discontinuities in the velocity field to avoid smoothing effects when averaging adjacent velocity vectors (e.g. for replacing outliers).

https://doi.org/10.5194/tc-2020-8
Preprint. Discussion started: 3 February 2020

When applying Eq. (5) over an area with a discontinuity in the velocity field, a step-like function occurring between two positions r_{i+1} and r_i with $r_i = (x_i, y_i)$ is replaced by a linear gradient (see above). As the interval Δr is decreased, the gradient increases. Hence, there is a numerical scaling effect: e.g. divergence and shear increase when calculated on grids of velocity vectors with higher spatial resolution. A discontinuity can be defined by a threshold for the difference of the velocities on both sides of it. The threshold depends on realistic values of velocity gradients in sea ice, and on the spatial resolution of the grid. The detection of possible discontinuities in a discrete field of velocity vectors, e.g. retrieved from SAR images, is helpful for the interpretation of the magnitudes of deformation.

3.8 Alternative method of analysis

In Sect. 2, the area-averaged velocity derivatives in a region are obtained by estimating contour integrals of the velocity around the boundary of the region. Two alternatives to this boundary integral ("BI") method are briefly discussed here: the least squares ("LS") method and the finite difference ("FD") method.

In the LS method, the velocity components u and v are modeled as linear functions of x and y, plus error. Suppose velocities (u_k, v_k) are given at locations (x_k, y_k) for $k = 1$ to n. The linear model is:

$$u_k = A + B\,x_k + C\,y_k + \varepsilon_k \tag{35a}$$

$$v_k = D + E\,x_k + F\,y_k + \delta_k \tag{35b}$$

where the constants A, B, C, D, E, F are chosen to minimize the variance of the errors ε_k and δ_k. The velocity derivatives u_x and u_y are then B and C, while v_x and v_y are E and F. The next step is to check whether the linear model accounts for a reasonable fraction of the variance in u_k and v_k by computing the squared correlation, and then whether the linear model does in fact provide a good fit to the data (by examining the spatial pattern of the errors ε_k and δ_k), or whether a quadratic or other non-linear model is more appropriate.

The FD method provides an estimate of u_x (and the other velocity derivatives) at a single point, based on Taylor series expansions of u and v about that point. For example, suppose we have velocities u_{k+1} and u_{k-1} at locations (x_{k+1}, y) and (x_{k-1}, y), where $x_k = x_0 + k\Delta x$. Then an estimate of u_x at (x_k, y) is:

$$u_x^{FD} = \frac{u_{k+1} - u_{k-1}}{2\Delta x} = \frac{u(x_k + \Delta x, y) - u(x_k - \Delta x, y)}{2\Delta x} = u_x + \frac{1}{6} u_{xxx} \Delta x^2 + O(\Delta x^4) \tag{36}$$

where the derivatives on the right-hand side are evaluated at (x_k, y). The first term on the right-hand side is the true value of u_x at (x_k, y); the rest of the terms are the truncation error, i.e. error = $u_x^{FD} - u_x = (1/6)\, u_{xxx}\, \Delta x^2$ + higher-order terms.

Hence, in summary, the three methods differ. The BI method provides area-averaged estimates of u_x, u_y, v_x, v_y. Application of the LS method results in the best linear models of u and v, from which u_x, u_y, v_x, v_y follow. From the FD method point estimates of u_x, u_y, v_x, v_y are obtained.

For a rectangular region with velocities given only at the four corners, it turns out that all three methods give the same estimates of u_x, u_y, v_x, v_y, assuming the FD estimate is made at the center of the rectangle. For a general configuration of points, the three methods give different estimates. Note that in the BI method, velocities inside the boundary of the region are ignored. In the LS method, velocities farther from the mean location $(\bar{x}, \bar{y})$ have greater weight in determining the slope of the linear model. The FD method is most appropriate for regularly-spaced square grids, whereas the BI and LS methods are equally applicable to irregular grids.

The LS method can be used as a diagnostic tool to determine whether the spatial resolution of the velocity data adequately captures the variability of the velocity field. Analysis of the spatial pattern of the LS residuals (errors) by standard

https://doi.org/10.5194/tc-2020-8
Preprint. Discussion started: 3 February 2020

methods (autocorrelation) reveals whether the linear velocity model is in fact a good fit to the velocity data or not. If it is a good fit, then the spatial resolution is adequate, and the truncation error in the BI method is small. If it is not a good fit and sufficient data are available, the region should be divided into smaller pieces and the calculation repeated for each piece. The BI method should be used to calculate the actual (area-averaged) velocity derivatives, since it does not depend on a model that needs to be checked for goodness of fit.

4. Conclusions

In this study we derived equations for calculating the magnitude of different deformation parameters within a given area, using displacement vectors retrieved from SAR images or buoy arrays. In the most general case, presented in Sect. 2.5, errors in measurements of position ("geolocation error"), velocity (determined from displacement), and area size have to be considered. Uncertainties in velocity and area size can be related to uncertainties in position measurements and (for velocity) time readings (Sects. 2.2 and 2.3). When retrieving displacements from pairs of SAR images a tracking error has to be considered additionally.

In Sect. 3, uncertainties of divergence and vorticity are derived based on the general equations introduced in Sect. 2, assuming squares and triangles as outlines for the area over which deformation is calculated. We chose these geometric shapes since they have been frequently used in past and recent studies of deformation in sea ice. The major findings are as follows.

- The equations reveal that the uncertainties in divergence and vorticity increase with the magnitudes of the velocity gradients, and with the geolocation and tracking errors. They decrease with increasing size of the area and the time interval ΔT used for calculating the velocity gradients (Sects. 3.4 and 3.5). Uncertainties of shear and total deformation are functions of divergence and vorticity and their uncertainties (Sect. 2.5).
- From several publications we concluded that the geolocation error in SAR images can be neglected in many cases, in particular for recent satellite missions. The same conclusion usually applies for errors in time readings of buoy positions and SAR image acquisitions, taking typical values of the time interval ΔT into account. For buoy arrays, the magnitude of the position error may not be negligible. Here, the reader is advised to check the manual for the position sensor and pay attention to whether the error is given as standard deviation or in another format.
- The tracking error that needs to be considered for displacement fields retrieved from SAR images is on the order of the length of one pixel or less, as several studies showed. A good approximation for the uncertainty of divergence and vorticity valid for a square with side L or a triangle with base L is $\sigma = a \times \sigma_{tr} / (\Delta T \times L)$, where $a = \sqrt{2}$ for the square and $a = 2$ for the triangle. If small windows are used for retrieving the displacement vectors, the ratio σ_{tr} / L and hence the uncertainty is large.
- The area uncertainty of the smallest possible ("elementary") cell, determined by the position of three or four adjacent displacement vectors at the edges of a triangle or square, is smaller than any combination of adjacent elementary cells with its outline covering more displacement vectors (Sect. 3.6). If, however, for an area of fixed size a variable number N of displacement vectors can be selected, the area uncertainty usually decreases with increasing N, and local variations on scales smaller than the area can be considered in more detail. For triangles, however, we found that the area uncertainty with 6 displacement vectors is larger than the one with three (see Sect. 3.6 for details).
- In Sects. 3.7 and 3.8 we provided thoughts concerning the validity of the derived equations, which assume that the velocity field inside elementary cells are continuous and can be approximated by a two-dimensional linear function. By including second-order terms or carrying out least-square fits over sub-regions of the velocity field, the validity of linearity can be judged. In the former case the second-order terms need to remain below a certain threshold, in the latter, the correlation coefficient should be large. Discontinuities in the velocity field should be detected before deformation is calculated to allow their impact to be assessed and to consider appropriate strategies to alleviate their impact.

https://doi.org/10.5194/tc-2020-8
Preprint. Discussion started: 3 February 2020

References

Berg, A., and Eriksson, L. E. B.: Investigations of a hybrid algorithm for sea ice drift measurements using synthetic aperture radar images, IEEE Trans. Geosci. Remote Sens., 52(8), 5023-5033, doi:10.1109/TGRS.2013.2286500, 2014.

Bevington, P. R., and Robinson, D. K.: Data reduction and error analysis for the physical sciences, 3rd edition, Mc Graw Hill, ISBN 0-07-247227-8, 2003.

Bouillon, S., and Rampal, P.: On producing sea ice deformation data sets from SAR-derived sea ice motion, The Cryosphere, 9, 663-673, doi:10.5194/tc-9-663-2015, 2015.

Cuffey, K. M., and Paterson, W. S. B.: The Physics of Glaciers, 4th edition, Academic Press, ISBN-10: 0123694612, 2010.

Demchev, D., Volkov, V., Kazakov, E., Alcantarilla, P. F., Sandven, S., and Khmeleva, V.: Sea ice drift tracking from sequential SAR images using accelerated-KAZE features, IEEE Trans. Geosc. Remote Sens., 55(9), 5174-5184, doi:10.1109/TGRS.2017.2703084, 2017.

Griebel, J., and Dierking, W., A method to improve high-resolution sea ice drift retrievals in the presence of deformation zones, Remote Sensing 9, 718, doi:10.3390/rs9070718, 2017.

Griebel, J., and Dierking, W.: Impact of sea ice drift retrieval errors, discretization, and grid type on calculations of ice deformation, Remote Sens., 10, 393, doi:10.3390/rs10030393, 2018.

Hollands, T., and Dierking, W. Performance of a multi-scale correlation algorithm for the estimation of sea ice drift from SAR images: initial results, Annals of Glaciology 52(57), 311-317, doi:10.3189/172756411795931462, 2011.

Hollands, T., Linow, S., and Dierking, W.: Reliability measures for sea ice motion retrieval from synthetic aperture radar images, IEEE J. Selected Topics in Applied Earth Observations and Remote Sensing, 8(1), 67-75, doi:10.1109/JSTARS.2014.2340572, 2015.

Holt, B., Rothrock, D. A., and Kwok, R.: Determination of sea ice motion from satellite images, in: Microwave Remote Sensing of Sea ice, edited by F. Carsey, Geophysical Monograph 68, American Geophysical Union, 343-354,1992.

Hutchings, J. K., and Hibler III, W. D.: Small-scale sea ice deformation in the Beaufort Sea seasonal ice zone, J. Geophys. Res. Oceans, 113, C08032, doi:10.1002/2006JC003971, 2008.

Hutchings, J. K., Roberts, A., Geiger, C. A., and Richter-Menge, J.: Spatial and temporal characterization of sea-ice deformation, Annals of Glaciology, 52(57), pp. 360-368, doi:10.3189/172756411795931769, 2011

Hutchings, J. K., Heil, P., Steer, A., and Hibler III, W. D.: Subsynoptic scale spatial variability of sea ice deformation in the western Weddell Sea during early summer, J. Geophys. Res., 117, C01002, doi:10.1029/2011JC006961, 2012.

Itkin, P., Spreen, G., Cheng, B., Doble, M., Gorard-Ardhuin, F., Haapala, J., Hughes, N., Kaleschke, L., Nicolaus, M., and Wilkinson, J.: Thin ice and storms: Sea ice deformation from buoy arrays deployed during N-ICE2015, J. Geophys. Res. Oceans, 122, 4661-4674, doi:10.1002/2016JC012403, 2017a.

Itkin, P., Spreen, G., Hvidgaard, S. M., Skourup, H., Wilkinson, J., Gerland, S., and Granskog, M. A.: Contribution of deformation to sea ice mass balance: a case study from an N-ICE2015 storm, Geophysical Research Letters 45, 789-796, doi:10.1002/2017 , 2017b.

Jansson, P., and Persson, C.-G., Uncertainty in area determination, Report, Royal Institute of Technology, Stockholm, Sweden ISBN 978-91-7595-350-2GL076056, 2014.

Karvonen, J.: Operational SAR-based sea ice drift monitoring over the Baltic Sea, Ocean Sci., 8, 473- 483, doi: 10.5194/os-8-473-2012, 2012.

Komarov, A. S., and Barber, D. G.: Sea ice motion tracking from sequential dual-pol RADARSAT-2 images, IEEE Trans. Geosci. Remote Sens., 52(1), 121-136, doi:10.1109/TGRS.2012.2236845, 2014.

Korosov, A. A., and Rampal, P., A combination of feature tracking and pattern matching with optimal parametrization for sea ice drift retrieval from SAR data, Remote Sensing, 9, 258, doi:10.3390/rs9030258, 2017.

Kræmer, T., Johnsen, H., and Brekke, C: Emulating Sentinel-1 Doppler radial ice drift measurements using Envisat ASAR data, IEEE Trans. Geosci. Remote Sens., 53(12), 6407-6418, doi:10.1109/TGRS.2015.2439044, 2015.

Kwok, R.: RGPS Arctic Ocean sea ice deformation from SAR ice motion: Linear kinematic features Winter 1996–1997, Winter 1997–1998, Summer 1998. Polar Remote Sensing Group, Jet Propulsion Laboratory Rep. JPL D-21524, 80 pp., 2003.

Kwok, R.: Contrasts in sea ice deformation and production in the Arctic seasonal and perennial ice zones, J. Geophys. Res., 111, C11S22, doi:10.1029/2005JC003246, 2006.

Lehtiranta, J., Siiriä, S., and Karvonen, J.: Comparing C- and L-band SAR images for sea ice motion estimation, The Cryosphere, 9, 357-366, doi:10.5194/tc-9-357-2015, 2015.

Leppäranta, M.: The drift of sea ice, 2nd edition, Springer Praxis Books in Geophysical Sciences, doi:10.1007/978-3-642-04683-4, 2011.

Lindsay, R. W.: Ice deformation near SHEBA, J. Geophys. Res., 107, C10, 8042, doi:10.1029/2000JC000445, 2002.

Lindsay, R. W., and Stern, H. L.: The RADARSAR Geophysical Processor System: Quality of sea ice trajectory and deformation estimates, J. Atmos. Ocean. Technol., 20, 1333-1347, 2003.

Linow, S., Hollands, T., and Dierking, W.: An assessment of the reliability of sea-ice motion and deformation retrieval using SAR images, Ann. Glaciol., 56, 69, doi:10.3189/2015AoG69A826, 2015.

Marsan, D., Stern, H., Lindsay, R., and Weiss, J.: Scale dependence and localization of the deformation of Arctic sea ice, Phys. Res. Lett., 17, doi:10.1103/PhysRevLett93.178501, 2004.

Muckenhuber, S., Korosov, A. A., and Sandven, S.: Open source feature-tracking algorithm for sea ice drift retrieval from Sentinel-1 SAR imagery, The Cryosphere, 10, 913-925, 2016

Rampal, P., Weiss, J., Marsan, D., and Bourgoin, M.: Arctic sea ice velocity field: General circulation and turbulent-like fluctuations, J. Geophys. Res., 114, C10014, doi:10.1029/2008JC005227, 2009.

Schubert, A., Jehle, M., Small, D., and Meier, E.: Geometric validation of TerraSAR-X high-resolution products, Proc. 3rd TerraSAR-X Science Team Meeting, Oberpfaffenhofen, Germany, 25-26 November, 2008.

Schubert, A., Miranda, N., Geudtner, D., and Small, D.: Sentinel-1A/B combined product geolocation accuracy, Remote Sensing, 9, 607, doi:10.3390/rs9060607, 2017.

Small, D., Rosich, B., Schubert, A., Meier, E., and Nüesch., D.: Geometric validation of low and high-resolution ASAR imagery, Proc. of the 2004 Envisat & ERS Symposium, Salzburg, Austria, 6-10 September 2004, ESA SP-572, 2005.

Stern, H. L., and Moritz, R. E.: Sea ice kinematics and surface properties from RADARSAT synthetic aperture radar during the SHEBA drift, J. Geophys. Res. Oceans, 107, C10, 8028, doi:10.1029/2000JC000472, 2002.

Thorndike, A. S.: Kinematics of sea ice, in: The Geophysics of Sea Ice, edited by N. Untersteiner, pp. 489-550, NATO ASI Series B: Physics vol. 146, Plenum Press, New York, 1986

https://doi.org/10.5194/tc-2020-8
Preprint. Discussion started: 3 February 2020

745 Websites:

[1] https://www.atomic-clock.galleon.eu.com

[2] https://sentinel.esa.int/web/sentinel/missions/sentinel-1/ground-segment/pod/egp

Code/Data availability: does not apply

750

Author contribution: WD and HS derived equations and discussed the validity of the approach, WD and JH collected and evaluated typical ranges of measurement parameters, all authors developed the concept of the study and worked on the text

Competing interests: none

https://doi.org/10.5194/tc-2020-8
Preprint. Discussion started: 3 February 2020

The Cryosphere Discussions
Open Access
EGU

755

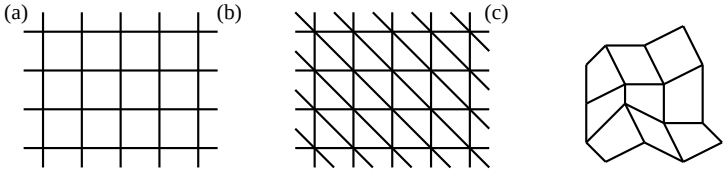

760

Figure 1: Different grids for displacement vectors: types (a) and (b) are fixed grid cells, (c) is an irregular grid in which cells change their shape from time step t_i to t_{i+1}.

765

https://doi.org/10.5194/tc-2020-8
Preprint. Discussion started: 3 February 2020

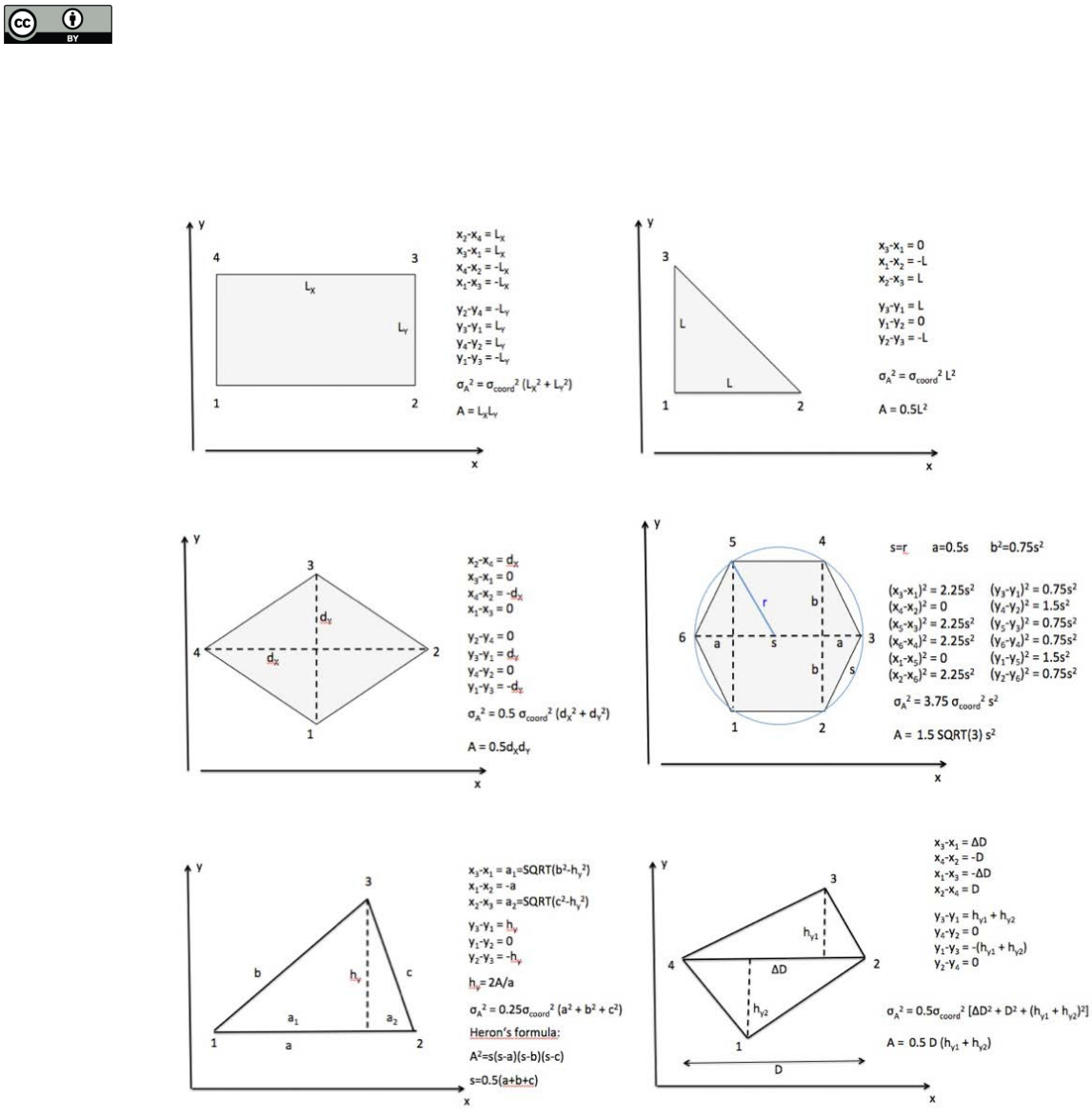

Figure 2: Application of Eq. (12) to different geometrical figures: rectangle, equal-sided right triangle, rhombus, regular hexagon, triangle, and quadrangle.

770

https://doi.org/10.5194/tc-2020-8
Preprint. Discussion started: 3 February 2020

The Cryosphere Discussions
Open Access
EGU

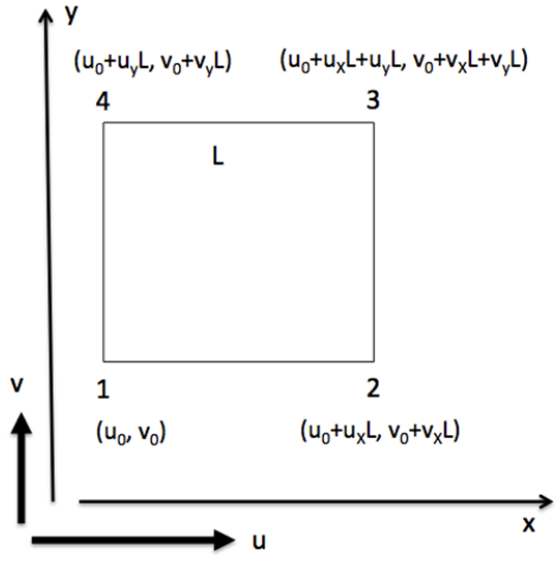

775

Figure 3. Uncertainty of divergence and vorticity for a square in a spatially varying velocity field with gradients u_x, u_y, v_x, v_y.

780

785

https://doi.org/10.5194/tc-2020-8
Preprint. Discussion started: 3 February 2020

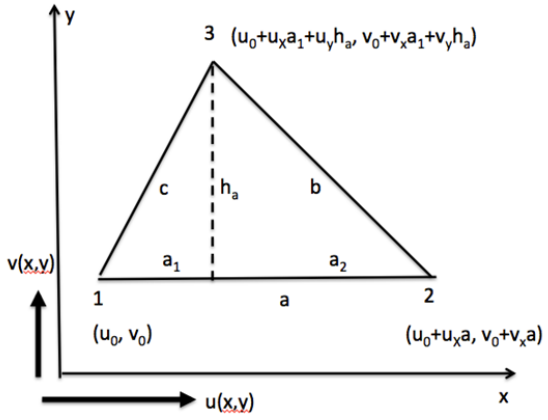

790 **Figure 4. Uncertainty of divergence for a triangle in a spatially varying velocity field with gradients u_x, u_y, v_x, v_y. The height h_a is $2A/a$ (A can be calculated from Heron's formula), and $a_1 = c^2-h_a^2$. Side a is the base of the triangle.**

https://doi.org/10.5194/tc-2020-8
Preprint. Discussion started: 3 February 2020

795

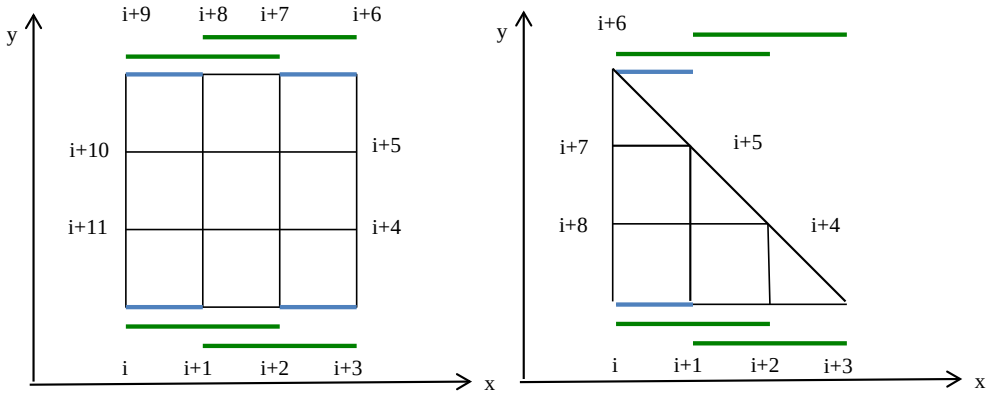

Figure 5: Derivation of equation 30 in *x*-direction for *N* = 3.

https://doi.org/10.5194/tc-2020-8
Preprint. Discussion started: 3 February 2020

800

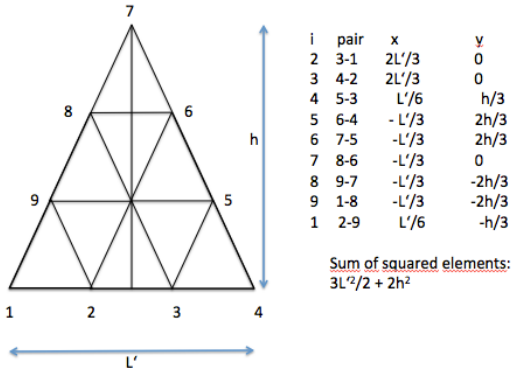

Figure 6. Application of Eq. (12) on a triangle with two equal sides for $N = 3$.

805